Research Square

Preprints are preliminary reports that have not undergone peer review.
They should not be considered conclusive, used to inform clinical practice,
or referenced by the media as validated information.

Seasonal water stress in a hyperhumid forest: evidence from multiple tree-ring variables and dekadal climate analysis

Hitoshi Yonenobu

yn@naruto-u.ac.jp

Naruto University of Education

Koh Yasue

Shinshu University

Yasuharu Hoshino

Nara National Research Institute for Cultural Properties

Motonari Ohyama

Tohoku University

Genki Katata

The Canon Institute for Global Studies

Research Article

Keywords: Japanese cedar, seasonal water stress, hyperhumid forest, dekadal analysis, climate--growth nonstationarity, soil water

Posted Date: October 23rd, 2026

DOI: https://doi.org/10.21203/rs.3.rs-11236760/v1

License: This work is licensed under a Creative Commons Attribution 4.0 International License.
Read Full License

Additional Declarations: No competing interests reported.

Seasonal water stress in a hyperhumid forest: evidence from multiple tree-ring variables and dekadal climate analysis

Hitoshi Yonenobu[1*], Koh Yasue[2], Yasuharu Hoshino[3], Motonari Ohyama[4], Genki Katata[5]

[1*]Graduate School of Education, Naruto University of Education, Naruto, 772-8502, Japan.
[2]Faculty of Agriculture, Shinshu University, Minami Minowa, 399-4598, Japan.
[3]Nara National Research Institute for Cultural Properties, Nara, 630-8577, Japan.
[4]Botanical Gardens, Tohoku University, Sendai, 980-0862, Japan.
[5]The Canon Institute for Global Studies, Tokyo, 100-6511, Japan.

*Corresponding author(s). E-mail(s): yn@naruto-u.ac.jp;

Key Message

In a hyperhumid cedar forest, antecedent summer soil water was consistently associated with ring width, while seasonal climate associations varied through time.

Abstract

Abundant annual rainfall need not exclude seasonal water constraints on tree growth. We examined this possibility in a natural Japanese cedar (*Cryptomeria japonica*) forest at Yanase, Japan, receiving more than 4000 mm of annual precipitation. Five width and density variables from the same 18 trees were related to station observations and locally evaluated gridded climate records. Monthly screening constrained subsequent dekadal analysis within 1950–2004. Previous-July modeled soil water was positively associated with earlywood and total width. Models also including cool-season temperature had standardized soil-water coefficients of 0.34–0.36 and adjusted $\boldsymbol{R^2 = 0.17}$–0.18. Coefficient directions were consistent across estimators and tree-resampling checks. Negative summer vapor-pressure-deficit correlations were compatible with water stress but did not pass multiplicity-adjusted screening. Latewood retained autumn and spring evaporation associations, whereas density responses were less consistent. Seasonal coefficients varied through time, with clearer period contrasts for radiation and atmospheric demand than for temperature and soil water. First-difference correlations with three external cedar chronologies ($\boldsymbol{r = 0.38}$–0.65) connected the local record to regional growth variability. The evidence supports a seasonal water-stress interpretation, conditional on climate-window and model selection. It does not partition the causal contributions of thermal and hydroclimatic influences or establish their physiological pathways. Antecedent summer conditions emerge as a recurring correlate of growth in this wet forest, alongside climate relationships that change across periods.

Keywords: Japanese cedar, seasonal water stress, hyperhumid forest, dekadal analysis, climate–growth nonstationarity, soil water

1 Introduction

More than 4000 mm of annual rainfall might seem to leave little scope for water to constrain forest growth. Yet rainfall reaches a tree through seasonally varying storage, drainage, and atmospheric demand. High vapor-pressure deficit (VPD) can restrict plant functioning even where precipitation is abundant (Grossiord et al. 2020). Recent observations in an everwet subtropical forest likewise identified soil moisture and evaporative demand as major controls of radial growth (Boeschoten et al. 2026). The question for humid-forest ecology is thus when water conditions matter, how their influence is recorded in wood, and whether the inferred relationships persist through time.

A ring integrates conditions during wood formation with influences carried over from preceding seasons. Its climatic associations can therefore differ in timing among width and density variables and can change over the life of a chronology. Such differences have been documented in multi-parameter analyses of Scots pine (Homfeld et al. 2025). In a very wet forest, they offer a way to examine whether seasonal water signals recur across features of the same rings. Agreement among paired variables strengthens the description of that signal, but does not constitute independent replication or identify the physiological mechanism responsible.

Tree rings can extend that question across decades, but the climatic record assigned to a forest is itself a source of uncertainty. A long station record may come from a different elevation or coastal setting; a gridded product represents an area rather than the rooting environment of sampled trees. Dataset choice and station distance can affect inferred tree-ring relationships (Tei et al. 2019). This problem is particularly relevant in steep terrain, where temperature, rainfall, and exposure can vary over short distances. Comparing the temporal behavior of available products, while retaining their distinct spatial and physical meanings, is therefore part of interpreting a climate–growth association.

Seasonal resolution matters as well. Monthly means can combine intervals with different water supply and atmospheric demand. Restricted dekadal (10-day) analysis provides a way to locate associations within broader monthly domains without searching arbitrary daily windows. Multiple ring variables then offer complementary views of the same climate history. Their use has clear precedents: earlywood and latewood in Japanese cedar (*Cryptomeria japonica*) already show different seasonal and previous-year associations (Hirano et al. 2021). Here, resolving width and density serves a more specific purpose: examining the timing and consistency of hydroclimatic signals in an exceptionally wet forest.

The unresolved issue is how to identify seasonal water constraints in very wet forests when climate records differ in local representativeness and growth sensitivities may vary through time. Interpretation therefore also depends on distinguishing a changing relationship from its cause. Thermal opportunity and water constraints can operate together, with their expression varying as climatic conditions and tree state change (Peltier and Ogle 2020). The divergence literature describes changes in the correspondence

between tree growth and temperature and considers several possible explanations (D'Arrigo et al. 2008). Temperature-induced drought is one causal hypothesis. A weakening temperature correlation alone cannot establish that pathway, nor show that one growth limitation has replaced another.

The natural cedar forest at Yanase, southeastern Shikoku, provides a particularly wet setting in which to ask whether abundant annual rain precludes seasonal water-stress signals in growth. Annual precipitation exceeds 4000 mm (Yamanaka 1954; Shikoku Regional Forest Office 2024), and a documented disc archive provides five width and density variables from the same 18 trees (Shikoku Regional Forest Office 2008; Yonenobu et al. 2021). A shared tree membership allows the seasonal evidence to be compared within one climate history. We combined Japan Meteorological Agency (JMA) observations, long-term Climatic Research Unit (CRU) records, and ERA5-Land fields, assessed their meteorological agreement, and compared local growth with independent regional cedar chronologies. The broader question concerns seasonal controls on growth in humid forests; the numerical climate responses are estimated for the Yanase archive. Three ecological expectations guided the interpretation.

H1: seasonal hydroclimatic sensitivity. Water supply and atmospheric demand can constrain growth even when annual rainfall is abundant. If these constraints are recorded in the rings, width should covary positively with soil water and negatively with atmospheric demand in current or antecedent seasons. Comparing width and density variables tests how consistently the seasonal associations appear across different features of wood formation.

H2: time-varying climate–growth relationships. Seasonal warmth can promote growth while water constraints restrict it, so their joint expression may depend on the climatic background and tree condition. We expected cool-season temperature and summer hydroclimatic associations to vary among periods, without requiring simultaneous changes or a discrete replacement of one limitation by another.

H3: regional growth coherence. If broad climatic variability contributes to Yanase growth, its interannual record should correlate positively with the independently assembled Yoshino, MGNS, and MGDO chronologies despite their contrasting site histories (Yonenobu et al. 2026; Ohyama et al. 2021). This comparison places a detailed local analysis within a wider ecological context while leaving the spatial applicability of its climate coefficients to be evaluated.

2 Materials and methods

2.1 Study design and analytical sequence

Supplementary methods, diagnostics, tables, and figures are provided in Online Resource 1.

This retrospective observational study uses 18 archived trees from one natural cedar stand. Its immediate inferential scope is the growth record represented by those trees over the stated analysis periods. Extrapolation to all trees in the stand or to other humid forests is not based on a probability sample of

either population. The broader ecological questions are evaluated through local climate associations and external chronology comparisons, with numerical coefficients retaining their local scope.

The three hypotheses address seasonal associations, change through time, and regional coherence. Their analyses differ in climate coverage and in the comparison needed to answer each question.

H1: seasonal hydroclimatic sensitivity. We compared station and gridded climate records, used monthly screening to define seasonal domains, and localized candidate associations at dekadal resolution. Fixed models for five ring variables then tested the selected associations within 1950–2004 (Sections 2.5–2.7). Temporal diagnostics, tree omission, and resampling evaluated their consistency; blocked and inverse verification assessed predictive performance and retained soil-water information (Sections 2.8–2.11). These checks address different properties of the same selected models.

H2: time-varying climate–growth relationships. We examined monthly and seasonal TRW associations with CRU over 1902–2004, then compared seasonal coefficients in separate modern TRW models over 1951–2004. Moving-window and period comparisons of the fixed component models supplied a further temporal check (Section 2.10). These analyses evaluate changing statistical relationships, without partitioning physiological causes.

H3: regional growth coherence. We compared the current X-ray TRW chronology with Yoshino, MGNS, and MGDO over 1902–2004, using both levels and first differences with block-bootstrap intervals (Section 2.12). A separate ocean–atmosphere analysis placed local climate windows in their meteorological context (Section 2.13); it did not test spatial transfer of the growth coefficients.

Trees provide within-stand subsamples for chronology construction and membership-sensitivity checks. The five ring variables are paired measurements, and the annual chronology values are temporally dependent observations; neither supplies independent replication among stands. External chronologies assess regional coherence rather than replicate the local climate–growth model. Complete-year rules and measurement sources are specified below and in Supplementary Table S13. Validation remains conditional on the preceding screening and model selection.

2.2 Study setting and sample provenance

The study stand (site code `39yn`) lies in the Yanase district of Kochi Prefecture, southeastern Shikoku, Japan (Fig. 1; representative position: 33.6674°N, 134.1341°E). It covers approximately 12.0 ha at 649–840 m a.s.l., with a mean elevation of 763 m. The stand occupies non-riparian terrain in the Higashigawa valley, within the upper Nahari River catchment upstream of Yanase Dam. Steep relief and frequent heavy rainfall characterize the catchment.

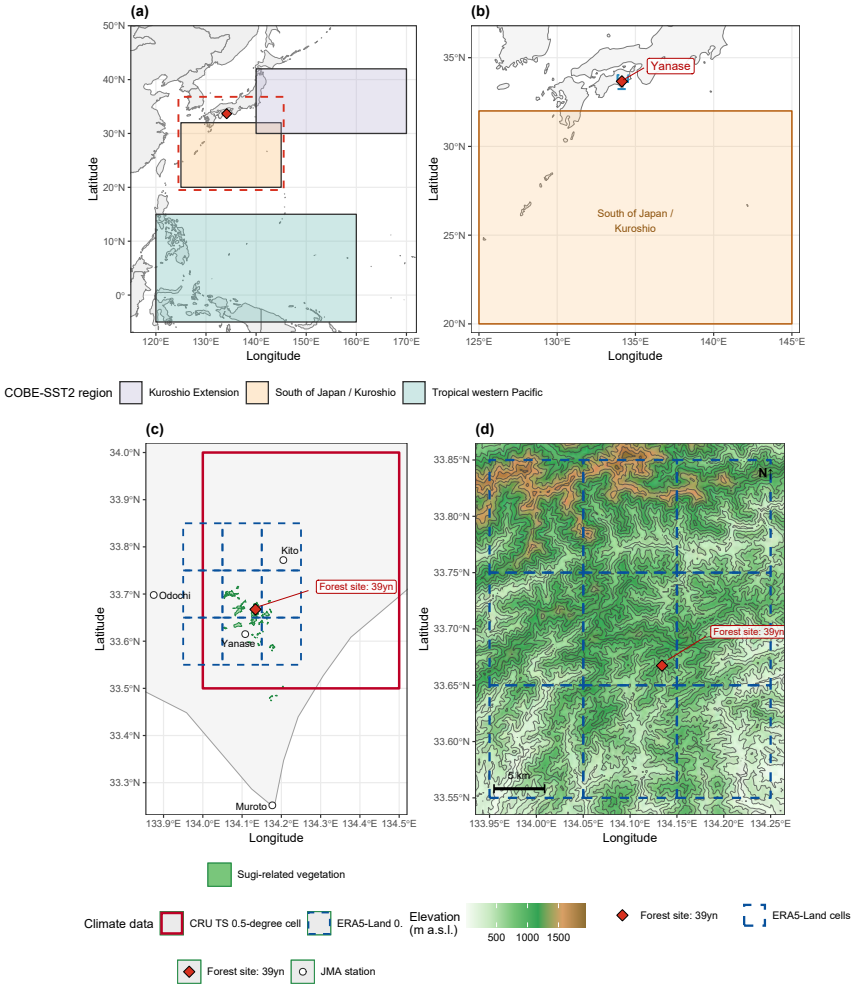


Fig. 1 Spatial setting of the Yanase study and climate-data domains. (a) Ocean–atmosphere context over Northeast Asia and the western North Pacific, showing the three fixed COBE-SST2 regional means; the dashed rectangle marks panel (b). (b) Western Japan and adjacent waters, showing forest site `39yn`, the South-of-Japan/Kuroshio region, and the extent enlarged in panel (c). (c) Sugi-related vegetation, the JMA stations at Yanase, Kito, Odochi, and Murotomisaki, the CRU TS 0.5-degree cell containing the site (the four-point interpolation support is specified in the Supplementary Material), the individual ERA5-Land 0.1-degree cells in the 3×3 averaging domain, and forest site `39yn`. (d) Elevation and contours across the complete ERA5-Land domain, with forest site `39yn`, the individual grid cells, a 5-km scale bar, and north orientation. Map lines delineate study areas and do not necessarily depict accepted national boundaries

Annual precipitation exceeds 4000 mm; we use "hyperhumid" to describe this precipitation regime (Yamanaka 1954; Shikoku Regional Forest Office 2024). The compartment is mapped predominantly as BC-type weakly dry Brown Forest Soil, with estimated soil thickness of 30–70 cm across most of its area (Forestry and Forest Products Research Institute 2026). These mapped attributes describe the stand setting. Rooting depth, plant-available water capacity, and access to bedrock or river water were not measured.

The wider Yanase landscape has a long history of regulated forest use under the Tosa Domain and entered national-forest administration in 1886 (Shikoku Regional Forest Office 2024). Conservation measures developed alongside timber production, including protected-forest designation during the Taisho period and cessation of natural Yanase-sugi harvesting in 2017. A mid-twentieth-century survey

documented cutting across the wider landscape and relatively natural vegetation in designated protected forest (Yamanaka 1954). The 2006–2008 Forestry Agency project identifies compartment 2032 i41 as the source of the present discs (Shikoku Regional Forest Office 2008). These records establish provenance and the history of regional stewardship, without establishing constant management or stand structure in the sampled compartment.

2.3 Tree-ring material and X-ray densitometry

All five ring metrics came from the same 18 stem discs used for the published Yanase width chronology (Yonenobu et al. 2021), collected in fiscal year 2006 from compartment 2032 i41 (Shikoku Regional Forest Office 2008). K. Yasue measured the X-ray profiles from which TRW, earlywood width (EWW), latewood width (LWW), mean ring density (MRD), and maximum density (MXD) were derived. The X-ray TRW chronology is identified as `39yn000_trw2026`. Crossdating used the optical chronology `39yn000_trw2021`, independently measured by Y. Hoshino (Yonenobu et al. 2021); the calendar assignments were then applied to all five metrics. The resulting series spanned 1713–2005. Fixed component models used 1950–2004, when all 18 trees and ERA5-Land overlapped. The longer CRU–TRW analyses used the archived optical-width chronology derived from the same discs, with the 16-year age-dependent spline as the primary standardization. Its raw values were checked against the optical measurement archive. The optical and X-ray records were kept distinct throughout the coordinate-sensitivity comparison.

For X-ray densitometry, radial samples prepared from the stem discs were boiled in distilled water for approximately 5 days and then extracted for approximately 5 days in a Soxhlet apparatus using a 2:1 toluene–ethanol mixture. The samples were mounted, cut parallel to the stem axis to approximately 1.6 mm thickness with a twin-blade saw, and conditioned for approximately 7 days at 20 °C and 60% relative humidity (equilibrium moisture content approximately 12%). Soft X-ray radiographs were obtained together with a standard absorber using a Softex EMBW custom-model system and Fuji IX-FR industrial X-ray film. The films were digitized with an EPSON GTX-970 scanner at 2400 dpi, and ring-width and density profiles were measured with WinDENDRO2009 (Hirano et al. 2020). Earlywood and latewood were separated at a density threshold of 0.55 g cm^{-3}. MRD was defined as the mean density across the complete annual ring, and MXD as the maximum density within the annual ring.

2.4 Chronology construction and standardization

Calendar-dated radial series were aggregated by tree before standardization and chronology averaging. For tree i, ring year t, and width metric $m \in \{\mathrm{EWW}, \mathrm{TRW}, \mathrm{LWW}\}$, raw width $\mathrm{rw}_{i,m,t}$ was divided by its fitted age-dependent trend $\widehat{\mathrm{rw}}^{\mathrm{trend}}_{i,m,t}$:

$$\mathrm{rwi}_{i,m,t} = \frac{\mathrm{rw}_{i,m,t}}{\widehat{\mathrm{rw}}^{\,\mathrm{trend}}_{i,m,t}}, \qquad m \in \{\mathrm{EWW}, \mathrm{TRW}, \mathrm{LWW}\}. \tag{1}$$

Here $\mathrm{rwi}_{i,m,t}$ is the dimensionless standardized width index for component m; when $m = \mathrm{TRW}$, it is the conventional ring-width index. The primary curve was an age-dependent spline with a nominal 16-year wavelength and a 0.5 frequency-response parameter.

For density metric $m \in \{\mathrm{MRD}, \mathrm{MXD}\}$, let $\mathrm{den}_{i,m,t}$ denote the raw annual density value. Density metrics were standardized within each tree as

$$\mathrm{denz}_{i,m,t} = \frac{\mathrm{den}_{i,m,t} - \overline{\mathrm{den}}_{i,m}}{s_{\mathrm{den},i,m}}, \qquad m \in \{\mathrm{MRD}, \mathrm{MXD}\}, \tag{2}$$

where $\overline{\mathrm{den}}_{i,m}$ and $s_{\mathrm{den},i,m}$ are the tree-specific mean and standard deviation.

Tree-level standardized series were aggregated by Tukey's biweight robust mean. To write one expression for all metrics, $\mathrm{series}_{i,m,t}$ denotes $\mathrm{rwi}_{i,m,t}$ for a width metric and $\mathrm{denz}_{i,m,t}$ for a density metric. For the values available in year t, the metric-specific chronology was

$$\mathrm{chron}_{m,t} = \mathrm{med}_{m,t} + \frac{\displaystyle\sum_{|u_{i,m,t}|<1} (\mathrm{series}_{i,m,t} - \mathrm{med}_{m,t}) \left(1 - u_{i,m,t}^2\right)^2}{\displaystyle\sum_{|u_{i,m,t}|<1} \left(1 - u_{i,m,t}^2\right)^2}, \tag{3}$$

with

$$u_{i,m,t} = \frac{\mathrm{series}_{i,m,t} - \mathrm{med}_{m,t}}{\kappa\, \mathrm{mad}_{m,t}}, \qquad \kappa = 9, \tag{4}$$

where $\mathrm{med}_{m,t}$ and $\mathrm{mad}_{m,t}$ are the annual median and median absolute deviation. Alternative detrending methods were retained for sensitivity analysis in the Supplementary Material.

Chronology quality was evaluated with sample depth and 51-year moving-window mean interseries correlation ($\bar{r}$). Annual subsample signal strength (SSS) was calculated separately as a descriptive replication diagnostic using a reference count of 18 tree-level curves and annual sample depth. The conventional SSS value 0.85 was retained only as a graphical and tabular reference and was not used to include or exclude a chronology. Primary climate-response screening used the standard biweight chronologies without prewhitening.

Width ratios and within-tree density z scores preserve variation on the respective measurement scales. Alternative age-dependent and fixed splines, supersmoothers, linear age terms, and additive density residuals were used to assess sensitivity to standardization. Primary methods were chosen on this measurement basis, without maximizing climate correlations; the full comparison is reported in the Supplementary Material.

2.5 Climate data and predictor construction

The climate products served different roles. JMA observations provided station references, CRU records supplied the longer 1902–2004 regional context, and ERA5-Land supplied atmospheric and modeled land-surface variables for the 1950–2004 analysis. Their differing spatial support, variable coverage, and overlapping periods were retained explicitly.

Station records came from Yanase, Kito, Odochi, and Muroto. Yanase supplied the closest precipitation record but no temperature record. Kito and Odochi supplied inland temperature, precipitation, and sunshine observations; the longer Muroto record added coastal humidity and vapor-pressure information. Muroto was an auxiliary regional reference, rather than a meteorological equivalent of the forest stand.

ERA5-Land (Muñoz-Sabater et al. 2021) was averaged over the nine grid points centered on 33.7°N, 134.1°E, the nearest grid point to the stand. The 3×3 neighborhood spans grid-point coordinates 33.6–33.8°N and 134.0–134.2°E; nearest-point extraction provided a sensitivity comparison. Meteorological agreement with JMA was evaluated over 1981–2004 using calendar-month anomalies, so that a shared seasonal cycle did not dominate the correlations. Raw-series mean differences assessed bias for commensurate variables. Solar radiation and sunshine duration were compared only as related quantities, using standardized anomalies. All 16 variable–station comparisons are summarized in Supplementary Table S14.

Screening included mean temperature, relative humidity, mean VPD, VPD at 14:00 Japan Standard Time (JST), precipitation, solar radiation, evaporation, precipitation minus evapotranspiration ($P - \mathrm{ET}$), and volumetric soil water in layers 1 and 2 (SWVL1 and SWVL2). Soil water and evaporation represent modeled land-surface conditions; neither was measured at the sampled trees. Accumulated total evaporation was converted from the native negative-upward water-equivalent convention to positive upward loss in mm. It includes transpiration and evaporation from other surfaces, and is not potential evapotranspiration. Daily aggregation used fixed JST (UTC+09:00). Figure 2 shows the common 1981–2005 dekadal climatology of ERA5-Land temperature and Yanase precipitation; this descriptive period differs from the 1981–2004 product-comparison interval.

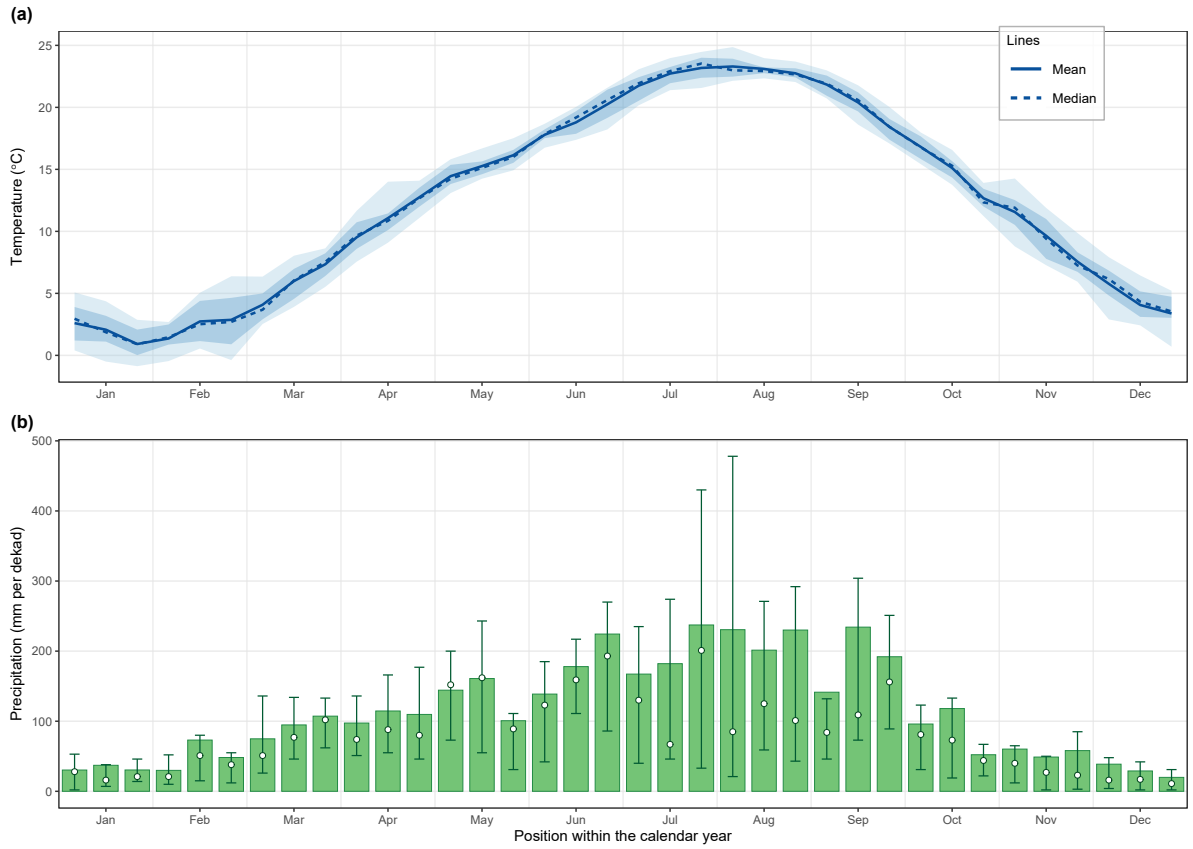


Fig. 2 Dekadal climatology of the Yanase environment during 1981–2005, the 25 complete years shared by the two datasets. (a) ERA5-Land 2-m air temperature averaged over the 3×3 grid-cell domain. Solid and dashed lines show the arithmetic mean and median, respectively; dark and light shading denote the interquartile and 10th–90th percentile ranges. (b) JMA Yanase precipitation. Bars show mean precipitation per dekad, open points show medians, and vertical intervals show the interquartile range. Temperature is drawn from ERA5-Land because Yanase has no temperature record. Fixed predictor windows and the complete monthly and dekadal response surfaces are reported in Fig. 4 and Supplementary Figs. S4–S7

CRU TS v4.09 was extracted by bilinear interpolation among four surrounding 0.5° grid points, with nearest-point extraction as a sensitivity comparison (Harris et al. 2020). We used the stand's representative coordinate, 33.6674°N, 134.1341°E, for 1901–2004; previous-year windows were then aligned with the 1902–2004 growth record. The corresponding scPDSI field, PET totals, approximate VPD, water balance, and temperature-adjusted PET residuals were derived from this extraction. The gridded estimates retain their regional spatial support. An extraction-coordinate sensitivity comparison is reported in Supplementary Table S15.

For the modern component models, climate windows extended from previous June through current October. Let $\mathrm{clim}_{t,d,j}$ denote the daily value of a generic meteorological variable on day j of dekad d, aligned to ring year t, and let $n_{t,d}^{\mathrm{day}}$ be the number of days in that dekad. Dekadal means were

$$\overline{\mathrm{clim}}_{t,d} = \frac{1}{n_{t,d}^{\mathrm{day}}} \sum_{j=1}^{n_{t,d}^{\mathrm{day}}} \mathrm{clim}_{t,d,j}, \tag{5}$$

and dekadal accumulations were

$$\mathrm{clim}^{\Sigma}_{t,d} = \sum_{j=1}^{n^{\mathrm{day}}_{t,d}} \mathrm{clim}_{t,d,j}. \tag{6}$$

Temperature, VPD, relative humidity, and soil water used Eq. 5; precipitation, evaporation, and radiation used Eq. 6. Each climate value was assigned explicitly to a ring year. Thus, July 1950 soil water was aligned with the 1951 ring, whereas April 1951 evaporation was aligned with the 1951 ring. In the equation notation, a prefix `p` identifies a previous-calendar-year window relative to ring year t.

2.6 Monthly screening and dekadal localization (H1)

A dekad comprises days 1–10, 11–20, or 21 through the end of a month. Monthly screening first identified broad seasonal domains. ERA5-Land dekadal analysis then localized associations within those domains while constraining the number of temporal choices. JMA–ERA5-Land response agreement was evaluated on monthly common-period records where comparable; it did not independently validate each selected dekad. No daily-window search was performed.

Cross-metric structure was evaluated for 1900–2004, and ERA5-Land response analyses were conducted for 1950–2004. Pearson correlations used an effective sample size correcting for first-order persistence:

$$n_{\mathrm{eff}} = n\,\frac{1-\rho_{1,\mathrm{clim}}\rho_{1,\mathrm{chron},m}}{1+\rho_{1,\mathrm{clim}}\rho_{1,\mathrm{chron},m}}, \tag{7}$$

where $\rho_{1,\mathrm{clim}}$ and $\rho_{1,\mathrm{chron},m}$ are the lag-1 autocorrelations of the climate series and the corresponding metric chronology. Benjamini–Hochberg (BH) false-discovery-rate (FDR) adjusted q values were reported for screening. Candidate promotion additionally used the directional and reproducibility criteria below; promotion did not require each localized correlation to pass an FDR threshold.

Domains retained across datasets and standardization sensitivities were localized using ERA5-Land. Candidate windows were evaluated by leave-one-decade-out analysis, monthly JMA–ERA5-Land agreement over common periods where comparable, and directional consistency. Thirty-six candidates met the promotion criteria and entered fixed-model comparison. Windows were held constant thereafter. The full set of localized candidates and promotion rules is reported in the Supplementary Material.

This hierarchy restricted the search within the observed record. Because screening and subsequent model diagnostics used the same record, the fixed models remained subject to selection uncertainty. The ocean–atmosphere extension likewise retained its defined context sources and seasons, using pathway-specific FDR values descriptively.

2.7 Fixed climate–growth models (H1)

The nominal component-model domain was 1950–2004. Candidate models for each metric were compared on years complete for that metric's full candidate predictor set: 1951–2004 ($n = 54$) for EWW, TRW, LWW, and MRD, and 1950–2004 ($n = 55$) for MXD. Previous-year predictors lacked a 1949 climate record, excluding ring year 1950 from the first four candidate sets. Responses and predictors were standardized on these common complete years for full-period model comparison. Temporal diagnostics used a different complete-case and scaling rule, detailed below and in Supplementary Table S13. For metric m, the general fixed climate–growth model was

$$\mathrm{chron}^{*}_{m,t} = \beta_{0,m} + \sum_{k=1}^{K_m} \beta_{k,m}\, \mathrm{clim}^{*}_{k,t} + \varepsilon_{m,t}, \tag{8}$$

where $\mathrm{chron}^{*}_{m,t}$ is the standardized metric chronology, $\mathrm{clim}^{*}_{k,t}$ is standardized local predictor k, and $\beta_{k,m}$ is therefore a standardized effect size.

Standardization puts coefficients on a common scale. Their environmental interpretation still depends on the variable: soil water integrates inputs, drainage, and evapotranspiration; evaporation reflects energy and surface moisture; VPD describes atmospheric demand.

For the width chronologies, $\mathrm{rwi}_{m,t}$ denotes the metric-specific Tukey-biweight width-index chronology before model-period z-standardization. The retained model was fitted separately to EWW and TRW:

$$\mathrm{rwi}^{*}_{m,t} = \beta_{0,m} + \beta_{1,m}\, \mathrm{swvl2}^{*}_{t,\mathrm{pJul3}} + \beta_{2,m}\, \mathrm{temp}^{*}_{t,\mathrm{Feb3}} + \varepsilon_{m,t}. \tag{9}$$

The selected LWW model was

$$\mathrm{rwi}^{*}_{\mathrm{LWW},t} = \beta_{0,\mathrm{LWW}} + \beta_{1,\mathrm{LWW}}\, \mathrm{evap}^{*}_{t,\mathrm{pOct3}} + \beta_{2,\mathrm{LWW}}\, \mathrm{evap}^{*}_{t,\mathrm{Apr1}} + \varepsilon_{\mathrm{LWW},t}. \tag{10}$$

The density models were

$$\mathrm{mrd}^{*}_{t} = \beta_{0,\mathrm{MRD}} + \beta_{1,\mathrm{MRD}}\, \mathrm{prec}^{*}_{t,\mathrm{Apr1}} + \varepsilon_{\mathrm{MRD},t}, \tag{11}$$

and

$$\mathrm{mxd}^{*}_{t} = \beta_{0,\mathrm{MXD}} + \beta_{1,\mathrm{MXD}}\, \mathrm{vpd}^{*}_{t,\mathrm{May1}} + \varepsilon_{\mathrm{MXD},t}. \tag{12}$$

The codes `pJul3`, `pOct3`, `Feb3`, `Apr1`, and `May1` specify the month and dekad, with `p` marking the previous calendar year.

Each model was estimated by OLS and by GLS-AR(1):

$$\varepsilon_{m,t} = \phi_m \varepsilon_{m,t-1} + \eta_{m,t}, \qquad \eta_{m,t} \sim \mathcal{N}(0, \sigma^2_{\eta,m}). \tag{13}$$

The GLS-AR(1) estimate was used to test whether an apparent climate effect persisted after serial dependence was represented explicitly. Effect uncertainty is reported as 95% confidence intervals (CIs), and predictor collinearity was evaluated with the variance inflation factor (VIF).

Model comparison used the small-sample corrected Akaike information criterion (AICc),

$$\mathrm{AICc} = -2\ell + 2k_{\mathrm{par}} + \frac{2k_{\mathrm{par}}(k_{\mathrm{par}}+1)}{n - k_{\mathrm{par}} - 1}, \tag{14}$$

where ℓ is the maximized log-likelihood and k_{par} is the number of estimated parameters.

Following Wasserstein and Lazar (2016), we interpreted P-values alongside coefficient magnitude and uncertainty. Evidence classes combined the screening results, agreement between OLS and GLS-AR(1), temporal sign retention, and blocked cross-validation. The labels "stable", "secondary", "weak/indeterminate", and "sign-unstable" summarize these diagnostics; their definitions are given in the Supplementary Material.

2.8 Blocked cross-validation

Six contiguous test blocks were used: 1950–1959, 1960–1969, 1970–1979, 1980–1989, 1990–1999, and 2000–2004. Models were refitted after withholding each block. Root-mean-square prediction error was summarized as

$$\mathrm{RMSE}_{\mathrm{CV},m} = \left[\frac{1}{n_{\mathrm{obs}}} \sum_{t=1}^{n_{\mathrm{obs}}} \left(\mathrm{chron}^*_{m,t} - \widehat{\mathrm{chron}}^*_{m,t,-b(t)} \right)^2 \right]^{1/2}, \tag{15}$$

where $\widehat{\mathrm{chron}}^*_{m,t,-b(t)}$ is the prediction for ring year t from the model trained without the temporal block $b(t)$ containing that year. Mean absolute error and prediction bias were calculated analogously.

Contiguous test blocks kept adjacent years together. The shorter 2000–2004 block allowed every complete observation to contribute a held-out prediction. For the 54-year models, the first block contained 1951–1959. Within each fold, scaling was estimated from the training years and applied to the test years. CV error contributed to model ranking alongside AICc, collinearity, and sign consistency. Scores therefore describe internal comparison and performance conditional on candidate selection; the full selection procedure was not evaluated in an independent outer validation loop.

2.9 Inverse soil-water verification

To compare the climate information retained by earlywood and total width, we also fitted inverse OLS models predicting previous-July ERA5-Land layer-2 soil water from either EWW or TRW alone. The

third-dekad and July-mean targets were examined over 1951–2004. Calibration on 1951–1977 was verified on 1978–2004, and the direction was then reversed. These inverse models also used six contiguous nine-year CV blocks, distinct from the growth-model blocks above. Predictor scaling used training years only. Verification correlation, reduction of error (RE), and coefficient of efficiency (CE) were calculated from held-out predictions. Definitions and the combined target and standardization criteria are given in the Supplementary Material.

2.10 Temporal analyses and model stability (H2)

The long-record analysis paired the optical TRW chronology with CRU climate over 1902–2004. Monthly associations covered previous May through current October; the six seasonal indices are defined in Supplementary Table S15. Pearson correlations for the 16-year age-dependent-spline chronology and bilinear climate extraction provided the primary summaries. Spearman correlations, alternative standardizations, and nearest-point extraction supplied sensitivity comparisons. Temporal variation was summarized with 51-year moving windows advanced in five-year steps, including the terminal window ending in 2004; 31- and 41-year windows provided sensitivity checks. Overlapping windows describe variation and are not independent period replicates.

Temporal change was also examined in two sets of modern models. The first used TRW for 1951–2004, with a baseline of previous-June precipitation and previous-November–current-March temperature. Radiation, VPD, and soil water were each added in a separate alternative model. GLS-AR(1) interactions compared 1951–1977 with 1978–2004. These monthly and seasonal predictors differ from the dekadal predictors in the five component models. Full definitions, coefficient orientation, nominal difference intervals, and sensitivity diagnostics are reported in the Supplementary Material and Table S12.

The second set used the fixed component models within 1950–2004, retaining years complete for each model's own predictors. This gave 54 years for the selected width models and 55 for the selected density models. Scaling used each response or predictor's available reference record within 1950–2004 and was held fixed across temporal windows. Thus, these reference fits need not equal the candidate-comparison fits, especially for MRD, whose temporal analysis additionally included 1950 (Supplementary Table S13).

The fixed models were refitted in 31-year moving windows. Early and late periods (1950–1977 and 1978–2004) were compared using

$$\mathrm{chron}^{*}_{m,t} = \beta_{0,m} + \sum_{k=1}^{K_m} \beta_{k,m}\,\mathrm{clim}^{*}_{k,t} + \gamma_m\,\mathrm{post}_t + \sum_{k=1}^{K_m} \delta_{k,m}\,\mathrm{clim}^{*}_{k,t}\mathrm{post}_t + \varepsilon_{m,t}. \tag{16}$$

where $\text{post}_t = 1$ in 1978–2004 and 0 otherwise. Continuous change was evaluated with

$$\text{chron}^*_{m,t} = \beta_{0,m} + \sum_{k=1}^{K_m} \beta_{k,m}\,\text{clim}^*_{k,t} + \lambda_m \tau_t + \sum_{k=1}^{K_m} \theta_{k,m}\,\text{clim}^*_{k,t}\tau_t + \varepsilon_{m,t}. \tag{17}$$

where $\tau_t = (t - 1977)/10$. All predictors and all predictor interactions entered together within a model; $\delta_{k,m}$ and $\theta_{k,m}$ describe the period contrast and per-decade change for predictor k. These are conditional changes with the other terms present.

For predictor k in metric m, rolling sign retention was

$$s^{\text{sign}}_{k,m} = \frac{1}{n_w} \sum_{w=1}^{n_w} \mathbb{I}\left[\text{sign}(\widehat{\beta}_{k,m,w}) = \text{sign}(\widehat{\beta}_{k,m,\text{full}})\right]. \tag{18}$$

A predictor was classified as sign-unstable when $s^{\text{sign}}_{k,m} < 0.80$ or when the interaction diagnostics supported a sign reversal. Weak coefficients and unsupported endpoint reversals were classified as weak or indeterminate rather than as confirmed regime shifts.

The same 31-year framework was applied to the fixed large-scale context pathways. Sign retention was evaluated separately for context–local and context–chronology links. A direct index–chronology relationship that lacked a stable context–local link was not promoted, even when its full-period coefficient had a small nominal P-value.

2.11 Metric-specific common signal and validation of fixed climate–growth estimates

The five metrics form a paired dataset from the same 18 trees. For each primary tree-level standardized metric, common-signal quality was calculated over the exact 1950–2004 model interval, during which all 18 tree series were represented in every year. Mean interseries correlation was the arithmetic mean of the 153 distinct pairwise correlations:

$$\bar{r}_{m,\text{model}} = \frac{2}{N(N-1)} \sum_{i<j} r_{ij,m}, \qquad N = 18. \tag{19}$$

For descriptive continuity with conventional chronology statistics, the corresponding model-interval EPS estimate was

$$\widehat{\text{EPS}}_{m,\text{model}} = \frac{N\bar{r}_{m,\text{model}}}{1 + (N-1)\bar{r}_{m,\text{model}}}. \tag{20}$$

Neither EPS nor the conventional value 0.85 was used to retain or reject a metric or climate model. The analysis instead kept internal common-signal strength separate from environmental and predictive validity.

Measurement and regional chronology comparisons are described in Section 2.12; additional crossdating diagnostics are reported in the Supplementary Material.

To assess sensitivity to tree membership, we omitted each of the 18 trees in turn, rebuilt the chronologies, and refitted the models by OLS and GLS-AR(1). We also sampled 18 tree identities with replacement in 2000 realizations, applying each draw to all five metrics to preserve their paired structure. Predictors, windows, and model structures were held fixed in both analyses. The resulting coefficient distributions describe sensitivity to the observed tree pool. They exclude uncertainty in the annual climate sequence and in the wider forest population.

Blocked predictive skill was expressed relative to the intercept-only model fitted within the same training fold:

$$R^2_{\mathrm{CV,null},m} = 1 - \frac{\sum_t \left(\mathrm{chron}^*_{m,t} - \widehat{\mathrm{chron}}^{*,\mathrm{selected}}_{m,t} \right)^2}{\sum_t \left(\mathrm{chron}^*_{m,t} - \widehat{\mathrm{chron}}^{*,\mathrm{null}}_{m,t} \right)^2}. \tag{21}$$

Positive values indicate lower held-out squared error than the fold-specific null prediction. Scores were calculated from the stored predictions for all held-out years, for each of the six folds, and after omitting one fold at a time, with the selected model held fixed.

2.12 Regional chronology coherence (H3)

Regional coherence was evaluated by comparing the current X-ray Yanase TRW chronology (`39yn000_trw2026`) with three published, species-specific external chronologies over their common 1902–2004 interval. The external records represented contrasting but independently assembled archives. The Yoshino regional chronology was developed from 60 provenance-screened, market-derived specimens from a centuries-long plantation system in western Japan (Yonenobu et al. 2026). The southern Tohoku comparison used two reference chronologies developed from old planted cedar avenues in Miyagi Prefecture: MGNS at the Sendai Castle Ninomaru avenue and MGDO at Daioji in Minamisanriku (Ohyama et al. 2021). For comparability, Yanase, Yoshino, MGNS, and MGDO were represented by harmonized 16-year age-dependent-spline chronologies.

Pearson correlations were calculated for chronology levels and first differences, with block-bootstrap 95% intervals (10-year blocks, 5000 replicates) to retain temporal dependence. The regional comparisons used 103 chronology-level and 102 first-difference observations. Optical and X-ray Yanase chronologies were compared separately to evaluate measurement reproducibility for the same trees. For this comparison we used harmonized 16- and 32-year age-dependent splines and raw-mean-curve crossdating diagnostics (Supplementary Material). The primary optical–X-ray comparison covered 1768–2004, with 237 chronology-level and 236 first-difference observations and the same bootstrap settings. The external chronologies tested regional common growth; spatial transfer of Yanase climate coefficients was outside this comparison.

2.13 Regional climate context

Regional sea-surface-temperature means and ocean–atmosphere indices were related to the local climate variables to examine their broader meteorological setting. The local climate–growth terms were held fixed during this analysis. Definitions, multiplicity handling, moving-window diagnostics, and pathway results are given in the Supplementary Material.

2.14 AI-assisted tools

During the preparation of this work, the authors used OpenAI ChatGPT and Codex to assist with English-language revision and with development, debugging, and verification of analysis scripts. Codex also assisted with figure layout corrections and the computational workflow used to regenerate Supplementary Figs. S10 and S11 from the corrected CRU extraction using existing R plotting scripts. After using these tools, the authors reviewed and edited the content as needed and take full responsibility for the content of the manuscript.

3 Results

The selected models identified previous-summer soil water as the most consistent seasonal width association (H1). Temporal contrasts differed among climate drivers (H2), and all three external chronologies shared interannual growth variability with Yanase (H3).

3.1 Meteorological agreement and local representation

Calendar-month anomalies agreed most closely for inland temperature ($r = 0.900$–0.968 across six station–variable pairs). Precipitation correlations were $r = 0.736$–0.746, while radiation–sunshine correlations were $r = 0.679$–0.734 (Supplementary Table S14). Agreement in variability coexisted with differences in magnitude: ERA5-Land mean monthly precipitation was 139 mm lower than at Yanase. The mean and median anomaly correlations across the 11 inland and Yanase comparisons were 0.841 and 0.900 for both nearest-point and 3×3 extraction after rounding. These results support using the products to examine common temporal variation while retaining their spatial and physical distinctions. The CRU extraction-coordinate comparison preserved the signs of all six primary seasonal TRW correlations, with a maximum absolute change in r of 0.018. Threshold crossings for some regional-context q values are documented with that comparison (Supplementary Table S15).

3.2 Chronology quality

The primary chronologies spanned 1713–2005 (Fig. 3), with all 18 trees represented in every year of the 1950–2004 component-model interval. Mean interseries correlation was 0.433 for EWW, 0.432 for TRW,

Table 1 Metric-specific common-signal quality over the shared 1950–2004 model interval and model-level blocked predictive skill. All five metrics were derived from the same 18 trees, and every tree was represented in every model year. Mean interseries correlation is the mean of 153 distinct tree-pair correlations. EPS is reported descriptively for continuity with chronology practice and is not used as a retention threshold. $R^2_{\mathrm{CV,null}}$ compares held-out squared error of the selected model with the fold-specific intercept-only model.

Metric	Primary standardization	Full span	Trees	$\bar{r}_{\mathrm{model}}$	$\widehat{\mathrm{EPS}}_{\mathrm{model}}$	$R^2_{\mathrm{CV,null}}$
EWW	Age-dependent spline, ratio	1713–2005	18	0.433	0.932	0.134
TRW	Age-dependent spline, ratio	1713–2005	18	0.432	0.932	0.138
LWW	Age-dependent spline, ratio	1713–2005	18	0.365	0.912	0.224
MRD	Within-tree z score	1713–2005	18	0.487	0.945	0.074
MXD	Within-tree z score	1713–2005	18	0.360	0.910	0.191

The full chronology span is 1713–2005 for every metric. Internal common-signal statistics and predictive skill answer different questions; their juxtaposition is intended to show, not collapse, those evidence domains. Longer-term moving-window $\bar{r}$, annual depth, and SSS are provided in the Supplementary Material. Common-signal statistics use all 55 years; CV uses 54 complete years for EWW, TRW, LWW, and MRD, and 55 for MXD (Supplementary Table S13).

0.365 for LWW, 0.487 for MRD, and 0.360 for MXD (Table 1). Optical and X-ray TRW measurements agreed closely at chronology level ($r = 0.974$, block-bootstrap 95% interval 0.950–0.989) and after first differencing ($r = 0.969$, 0.945–0.984) over 1768–2004 (Supplementary Table S8).

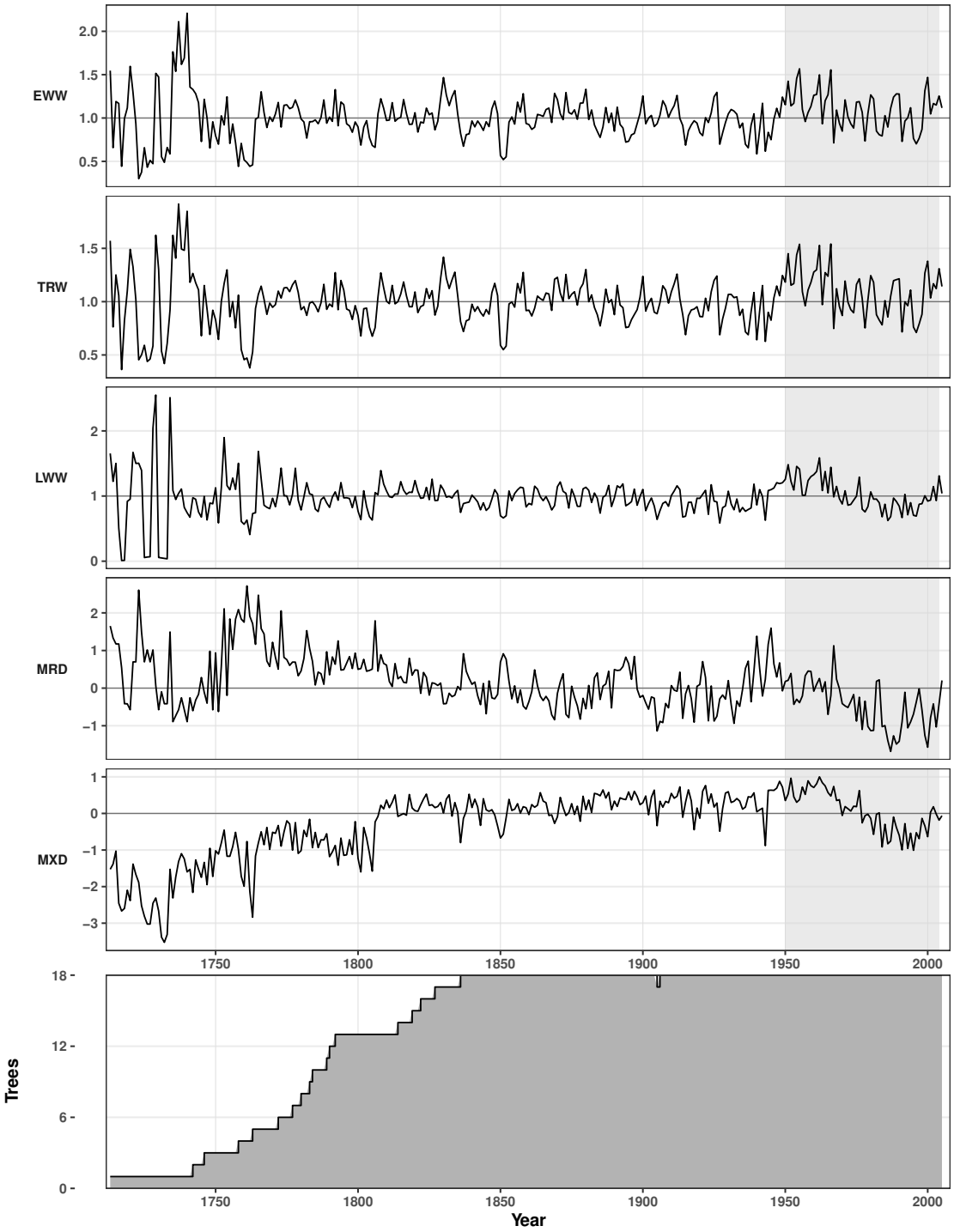


Fig. 3 Primary annual chronologies derived from the common 18-disc Yanase measurement set for 1713–2005. The upper five panels show the Tukey-biweight EWW, TRW, LWW, MRD, and MXD chronologies in fixed order; the lower panel shows the common tree-level sample depth. The shaded interval identifies 1950–2004, the period used for the fixed climate–growth models

3.3 Seasonal hydroclimatic associations

The H1 analysis localized the most consistent width association with soil water to the third dekad of previous July. Layer-2 ERA5-Land soil water was positively associated with both EWW and TRW over their 1951–2004 complete-year interval. For EWW, the selected model had an adjusted R^2 of 0.168 and similar soil-water coefficients under OLS and GLS-AR(1) ($\beta = 0.34$–0.35). The TRW coefficient was 0.35–0.36, with adjusted $R^2 = 0.180$. Close covariation between the two width metrics indicated that earlywood carried much of the annual-width signal. Within the same broad summer domain, EWW was negatively correlated with mean and afternoon VPD in the second dekad of previous July ($r = -0.324$ and -0.333). These were descriptive localized candidates (BH $q = 0.421$ for both), not independent confirmations of the selected soil-water effect. The weaker positive temperature association was localized to the third dekad of current February.

Latewood retained two distinct evaporation windows: the third dekad of previous October and the first dekad of current April. Together they yielded adjusted $R^2 = 0.202$, with a maximum VIF of 1.05. Both terms retained their expected directions across estimators and temporal diagnostics. Their limited collinearity showed that the autumn and spring windows supplied different information within the fitted model.

Density responses were less consistent. The MRD association with first-dekad April precipitation was positive under OLS ($\beta = 0.305$, 95% CI: 0.040–0.570) and GLS-AR(1) ($\beta = 0.182$, 0.007–0.357) in the 54-year candidate-comparison fit. The 55-year temporal reference fit retained a positive GLS-AR(1) coefficient ($\beta = 0.169$), but its interval included zero (-0.001–0.339). The MRD association was therefore modest and sensitive to the analysis frame (Supplementary Table S13). By contrast, the first-dekad May MXD–VPD coefficient changed sign between estimators and repeatedly reversed in moving windows. Dekadal localization therefore separated seasonal associations of differing robustness (Table 2; Figs. 4–5).

Table 2 Fixed climate–growth effects for 1950–2004. Coefficients are standardized ordinary least squares (OLS) and generalized least squares with first-order autoregressive residuals (GLS-AR(1)) estimates; continuous model-compatibility P values are given in parentheses. Tree-membership sensitivity summarizes 18 single-tree omissions and 2000 paired tree-resampling realizations. Model-level predictive skill is reported once per metric in Table 1 and in full in Supplementary Table S10.

Response	Local meteorological window	OLS β (P)	GLS-AR(1) β (P)	Temporal evidence	Tree membership	Role
EWW	Previous July dekad 3 SWVL2	0.344 (0.009)	0.343 (0.003)	Stable predictor	Robust	Core
EWW	Current February dekad 3 temperature	0.230 (0.077)	0.167 (0.159)	Weak / indeterminate	Robust	Model covariate
TRW	Previous July dekad 3 SWVL2	0.346 (0.008)	0.354 (0.002)	Stable predictor	Robust	Shared signal
TRW	Current February dekad 3 temperature	0.247 (0.056)	0.182 (0.113)	Weak / indeterminate	Robust	Model covariate
LWW	Previous October dekad 3 evaporation	0.288 (0.026)	0.235 (0.009)	Stable	Robust	Core
LWW	Current April dekad 1 evaporation	0.327 (0.012)	0.254 (0.009)	Stable	Robust	Core
MRD	Current April dekad 1 precipitation	0.305 (0.025)	0.182 (0.041)	Stable, modest	Robust	Secondary
MXD	Current May dekad 1 VPD	−0.402 (0.002)	0.066 (0.361)	Sign-unstable	Varies by estimator	Limitation

"Robust" denotes retention of the full-sample coefficient sign after every single-tree omission and across all paired tree-resampling realizations under both estimators. The MXD coefficient is classified separately because OLS and GLS-AR(1) support opposite directions. Coefficients use the candidate- comparison years (54 for EWW, TRW, LWW, and MRD; 55 for MXD). Temporal diagnostics use model-specific years and reference scaling. For MRD, the 55-year temporal reference GLS-AR(1) interval includes zero, although its 54-year comparison interval does not (Supplementary Table S13).

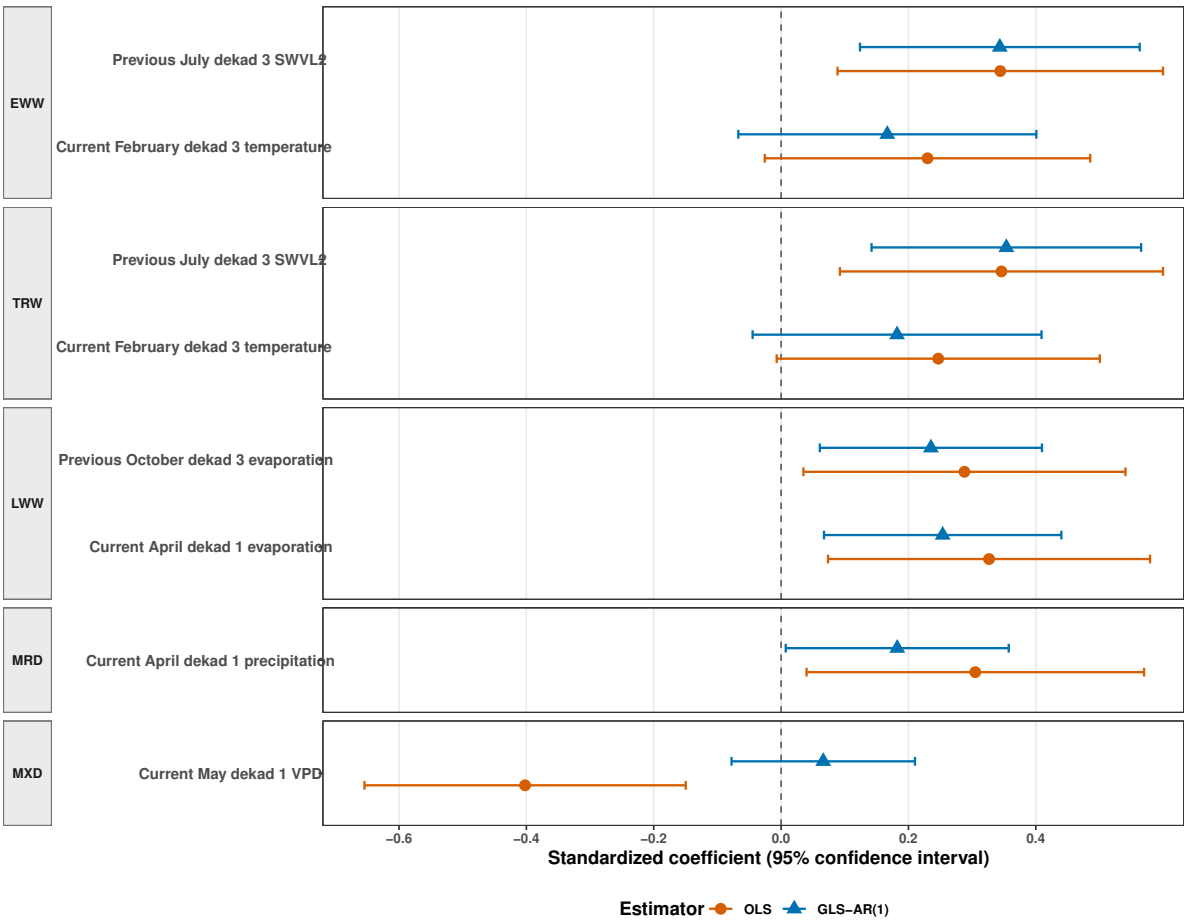


Fig. 4 Standardized coefficients and 95% confidence intervals for the retained component-resolved climate–growth models fitted over 1950–2004. OLS and GLS-AR(1) estimates are shown together for each fixed predictor. Previous-July soil water for EWW and TRW, both LWW evaporation terms, and current-April precipitation for MRD retained their expected directions across estimators, whereas the May VPD effect on MXD changed sign and had an interval spanning zero under GLS-AR(1)

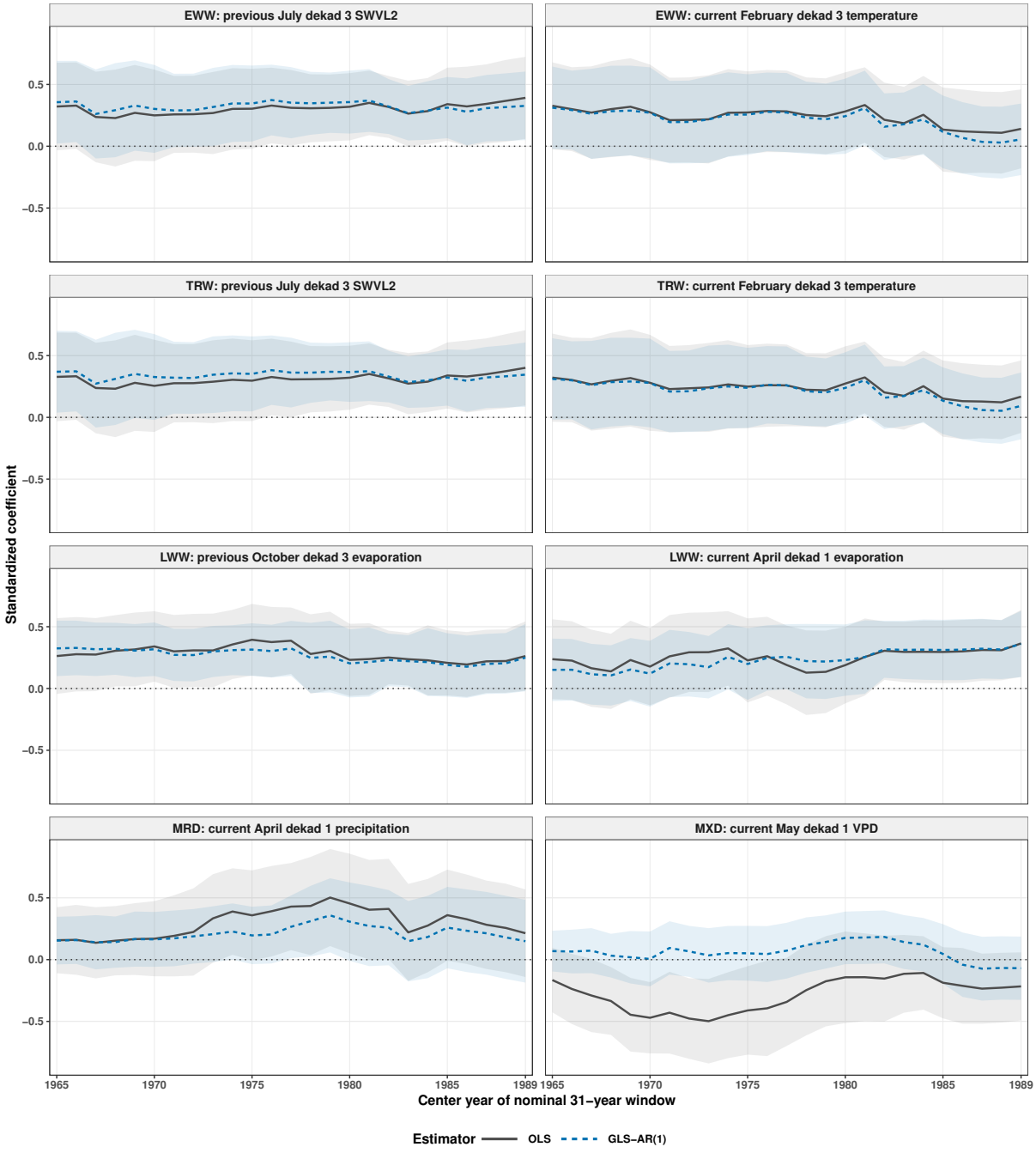


Fig. 5 Temporal stability of the selected climate–growth coefficients in 31-year moving windows. Predictors and responses were standardized with the full-period 1950–2004 scaling before each window was fitted. Previous-July soil water for EWW and TRW, previous-October and current-April evaporation for LWW, and current-April precipitation for MRD retained their expected signs in the required fraction of windows. The May VPD coefficient for MXD repeatedly changed sign, supporting its classification as temporally unstable

3.4 Climate–growth relationships varied through time

Over the longer 1902–2004 optical TRW record, positive correlations were observed with winter–early-spring temperature ($r = 0.324$), previous-summer scPDSI ($r = 0.346$), and previous-summer climatic water balance ($r = 0.324$). Thus, thermal and hydroclimatic associations coexisted in the long record. In 51-year moving windows, the oriented previous-June precipitation correlation increased descriptively from 0.114 in the earliest window to 0.367 in the latest.

Modern seasonal models resolved additional temporal variation (Supplementary Table S12). Between 1951–1977 and 1978–2004, the expected-direction temperature coefficient declined from 0.398 to 0.148, while the soil-water coefficient increased from 0.119 to 0.372. Radiation and VPD coefficients changed direction, and their nominal 95% difference intervals excluded zero. These contrasts support H2 at the level of changing statistical relationships. They came from separate alternative models and are conditional on their predictor covariance, without adjustment for multiple comparisons or selection.

The temperature and soil-water patterns persisted across nearby period boundaries but were sensitive to individual years or five-year blocks; their difference intervals included zero. The evidence therefore differs among drivers. The fixed split is a temporal comparison, and the archived structural diagnostics supplied no breakpoint estimate identifying a transition year.

3.5 Sensitivity to tree membership and predictive performance

The retained EWW, TRW, LWW, and MRD effects preserved their expected signs when individual trees were omitted and in paired tree resampling. The MXD result remained unstable. Alternative standardizations also preserved the principal interannual-to-subdecadal associations.

Inverse tests showed a narrower difference between earlywood and total width (Supplementary Table S11). For previous-July third-dekad soil water, EWW retained positive coefficient of efficiency (CE) in both fixed calibration directions (0.161 and 0.024); TRW failed the late-to-early direction (CE=−0.095). Blocked-CV CE, however, was almost identical: 0.084 for EWW and 0.085 for TRW. Earlywood met the positive-CE criterion in both fixed directions, without a corresponding gain in blocked prediction. These diagnostics do not test a statistically significant difference in skill between the two metrics. July-mean skill was weaker, and only EWW met the combined criteria for the two soil-water targets and standardization sensitivity. The broader July–April $P - \mathrm{PET}$ target failed level transferability tests, precluding its use here as a historical reconstruction.

3.6 Regional growth coherence and climate context

Regional coherence was strongest with Yoshino. Over 1902–2004, its chronology-level correlation with Yanase was $r = 0.570$ (0.370–0.732), and the first-difference correlation was $r = 0.646$ (0.486–0.764). Corresponding values were $r = 0.233$ (0.035–0.414) and $r = 0.411$ (0.208–0.565) for MGDO, and $r = 0.092$

(−0.153–0.371) and $r = 0.377$ (0.208–0.518) for MGNS. All three first-difference intervals excluded zero, supporting the H3 expectation of shared interannual growth. Coherence at chronology level was more variable, particularly for MGNS.

The secondary ocean–atmosphere analysis placed these local associations in their regional meteorological context. Large-scale variability was expressed mainly through variables already represented in the local models (Supplementary Figs. S12–S13 and Table S7).

4 Discussion

4.1 Seasonal water-stress signals despite abundant rainfall

Yanase shows why annual rainfall alone is an incomplete guide to the water conditions relevant to growth. Width was positively associated with previous-July soil water, while negative VPD associations occupied the same broad summer domain. A weaker cool-season temperature association coexisted with these hydroclimatic signals. The evidence is consistent with seasonal water constraints in a forest receiving more than 4000 mm of annual rain. It does not require the stand to experience a persistently dry climate.

The most consistent model evidence came from width. The selected soil-water coefficients retained their direction across estimators, temporal windows, and tree-composition tests. Negative summer VPD correlations add a physically compatible observation, although their screening q values did not pass the FDR threshold used to mark the response surfaces. We therefore interpret the convergence as support for the H1 hypothesis, conditional on selection, rather than as independent physiological proof. Atmospheric demand and soil water can jointly affect tree functioning (Grossiord et al. 2020). Direct observations in another everwet forest also implicate both variables in radial growth (Boeschoten et al. 2026); the Yanase archive extends the temporal perspective through historical climate–growth associations.

Terrain provides a plausible setting for seasonal differences between rainfall and water available to trees. The stand occupies non-riparian slopes, with mapped BC-type soil and estimated soil thickness of 30–70 cm. Drainage and limited storage could matter between rainfall events, but those mapped attributes do not quantify rooting depth or plant-available water. Previous-summer associations could also involve carry-over effects on tree condition or stored resources. Resolving these pathways requires observations of the trees and their rooting environment.

The other ring variables refine the seasonal picture without all carrying equally strong drought evidence. Latewood retained previous-October and current-April evaporation terms; mean density added a modest spring-precipitation association, and maximum density was unstable. Positive actual-evaporation coefficients cannot be read as stronger drought effects: evaporation depends on both energy and available water and includes fluxes from several surfaces. H1 consequently receives its clearest support from the summer soil-water and width relationships.

4.2 What local climate evaluation and dekadal analysis contribute

Assigning climate to a mountain forest requires more than choosing the nearest available record. JMA observations constrain what can be learned from gridded products, CRU supplies a long regional perspective, and ERA5-Land provides the finer temporal resolution and land-surface variables needed for the local models. The high temperature-anomaly correlations and lower precipitation agreement show why those roles should remain distinct. Yanase precipitation, in particular, exceeded the ERA5-Land mean despite their common temporal variation. Neither correlation nor spatial averaging removes that difference.

Dataset sensitivity is an established tree-ring concern (Tei et al. 2019). Here, the product comparison makes the basis of local interpretation explicit: common monthly behavior supports the seasonal domains, but coastal humidity does not directly validate humidity at the stand, and meteorological agreement does not validate modeled root-zone water. CRU was extracted at the stand coordinate, but its 0.5-degree source grid still represents a broader area. Geographical alignment improves consistency of the analysis without making a gridded estimate equivalent to conditions experienced by the trees.

Within that framework, restricted dekadal analysis distinguished late-July soil water from autumn and spring evaporation associations. The two latewood windows had little collinearity and contributed different information to the fitted model. Five ring variables allowed the same candidate seasons to be examined from several measurement perspectives, including the inconsistent maximum-density result. Earlywood and latewood analysis itself is well established (Hirano et al. 2021); its value here lies in this assessment of hydroclimatic timing and consistency under very wet conditions. The selected dekads are statistical windows, not observed dates of cambial activity or wood formation. Their apparent precision should be tested against phenological observations.

4.3 Changing interplay of thermal and hydroclimatic influences

The observed temporal changes in climate–growth relationships are consistent with a changing interplay of thermal and hydroclimatic influences in this hyperhumid forest. Their relative causal contributions were not quantified here. These findings highlight the need to evaluate whether climate sensitivities inferred from one period remain applicable under different climatic conditions.

This interpretation accommodates the coexistence of temperature and water-related associations in the long record and the unequal changes among seasonal coefficients. It does not require a thermal limitation to cease before a water constraint can become consequential. Radiation and VPD provided the clearest period contrasts; the temperature and soil-water differences were less well resolved. Because the summer variables entered separate alternative models, the coefficients cannot be interpreted as proportions of a common causal total. Changing predictor covariance, tree condition, and stand structure can also affect their values (Peltier and Ogle 2020).

The distinction matters when discussing divergence. A changing temperature–growth correspondence is a pattern requiring explanation, whereas temperature-induced drought specifies a pathway (D'Arrigo et al. 2008). Warming could increase atmospheric demand or alter soil-water conditions, but the present coefficient comparisons do not isolate those links. In particular, the temporal VPD contrast comes from a separate seasonal model and cannot by itself be read as evidence of increasing atmospheric water stress. Retaining several plausible influences is more consistent with these observations than assigning the forest a discrete new limitation regime.

The Yoshino plantation archive also raises questions about changing hydroclimatic sensitivity (Yonenobu et al. 2026). Its forest history differs from natural Yanase cedar, so their comparison does not identify a management effect or a shared rate of change. Both records motivate evaluation of climate relationships over the intended period of application. Neither fixes a future trajectory.

4.4 Regional relevance of a detailed local study

Positive first-difference correlations with Yoshino, MGNS, and MGDO support H3 and place Yanase within broader annual cedar-growth variability. Coherence was strongest with Yoshino, while weaker chronology-level correlations with southern Tohoku indicate differences at longer timescales. The ocean–atmosphere analysis provides a second form of context by relating regional variability to the local climate windows. These comparisons connect the stand to regional growth and meteorological variation without equating the two forms of evidence.

Yanase allows a close examination of seasonal water constraints within a very wet climate. Holding tree membership and climate history in common makes differences among ring variables interpretable within that setting; it does not increase the number of independent forest sites. The broader inference concerns a process hypothesis: seasonal water supply and demand may remain relevant to growth where annual precipitation is high. Assessing its prevalence requires observations across forests. Neither the paired ring measurements nor external chronology correlations establish that Yanase coefficients or exact seasonal windows apply elsewhere.

4.5 Robustness, prediction, and limits of inference

Inverse soil-water tests gave positive verification CE for earlywood in both fixed calibration directions (0.161 and 0.024), whereas total width failed one direction. Their blocked-CV scores were nevertheless almost identical (0.084 and 0.085). Thus, temporal consistency and predictive performance provide different checks on the seasonal signal; these results do not demonstrate a general predictive advantage of earlywood. The broader July–April water-balance target failed level transferability tests, so the seasonal associations do not justify a single historical drought reconstruction.

Total width contains earlywood and latewood by definition, and agreement among these metrics is not independent replication. Tree omission and resampling quantify sensitivity to membership within the archive; they cannot remove confounding by age, competition, or changes in stand structure. The management records establish provenance and regional stewardship history, without documenting an unchanged sampled compartment.

Candidate screening and model ranking reused the available climate record, and chronology construction used the full ring record. Reported intervals and validation scores therefore omit the full uncertainty of selection. Formal tests of incremental information or differences in predictive skill were not performed. Physiological attribution would require direct measurements of soil-water potential, rooting, sap flow, canopy water status, and cambial phenology. The climate analyses end in 2004 and do not characterize subsequent decades.

4.6 Implications for understanding growth in humid forests

The preceding-summer soil-water association raises a question about how conditions before ring formation are carried into subsequent growth. The annual records locate this association in time; they cannot distinguish effects on stored resources, foliage, roots, or other aspects of tree condition. Concurrent measurements of soil-water potential, canopy water status, and cambial activity would help test those pathways. For latewood, observations extending into autumn and early spring would allow the evaporation associations to be evaluated against the timing of wood formation.

The changing seasonal coefficients also caution against assigning a tree or stand a single, permanent climatic limitation. Temperature and water-related influences can coexist, while their statistical expression varies with the period examined. This interpretation remains compatible with several physiological pathways and with changes in predictor covariance or stand conditions. It provides a basis for asking which processes change, without treating a correlation shift as a diagnosis of temperature-induced drought.

5 Conclusions

Annual rainfall exceeding 4000 mm did not preclude growth associations consistent with seasonal water stress at Yanase. The most consistent width signal concerned soil water in the preceding summer. Locally evaluated climate records and restricted dekadal analysis helped locate that signal, while the paired ring variables distinguished other seasonal associations and less consistent responses. Thermal and hydroclimatic relationships changed through time, with the clearest period contrasts for radiation and atmospheric demand. These patterns support a changing expression of coexisting climatic influences; they do not quantify their causal shares or establish a switch between limitation regimes. Regional growth coherence places the Yanase record in a broader context, but its coefficients and precise seasonal windows

retain their local scope. The study identifies antecedent summer water conditions as a specific target for testing how growth responds to seasonal climate in very wet forests.

Supplementary information

Online Resource 1. Supplementary methods, chronology diagnostics, seasonal climate-response analyses, model checks, regional comparisons, and CRU coordinate-sensitivity results (Supplementary Tables S1–S15 and Figs. S1–S17), with an abbreviations and notation glossary.

References

Boeschoten LE, Smith-Martin CM, Medina-Vega JA, et al (2026) Water limits radial tree growth more than light in an everwet subtropical forest. Global Change Biology 32(7):e71021. https://doi.org/10.1111/gcb.71021

D'Arrigo R, Wilson R, Liepert B, et al (2008) On the 'divergence problem' in northern forests: A review of the tree-ring evidence and possible causes. Global and Planetary Change 60(3–4):289–305. https://doi.org/10.1016/j.gloplacha.2007.03.004

Forestry and Forest Products Research Institute (2026) Forest soil digital map. https://www2.ffpri.go.jp/soilmap/index.html, accessed 4 September 2026; soil type and estimated soil thickness are map-derived attributes

Grossiord C, Buckley TN, Cernusak LA, et al (2020) Plant responses to rising vapor pressure deficit. New Phytologist 226(6):1550–1566. https://doi.org/10.1111/nph.16485

Harris I, Osborn TJ, Jones P, et al (2020) Version 4 of the CRU TS monthly high-resolution gridded multivariate climate dataset. Scientific Data 7:109. https://doi.org/10.1038/s41597-020-0453-3

Hirano Y, Saitoh TM, Fukatsu E, et al (2020) Effects of climate factors on the tree-ring structure of Cryptomeria japonica in central Japan. Mokuzai Gakkaishi 66(3):117–127. https://doi.org/10.2488/jwrs.66.117

Hirano Y, Saitoh TM, Fukatsu E, et al (2021) Relationships among radial growth of Cryptomeria japonica, carbon budget of a forest ecosystem, and climate factors in a cool temperate zone. Mokuzai Gakkaishi 67(3):117–128. https://doi.org/10.2488/jwrs.67.117

Homfeld IK, Reinig F, Martinez del Castillo E, et al (2025) Beyond maximum density: multi-parameter insights into Scots pine climate sensitivity. Trees 39:101. https://doi.org/10.1007/s00468-025-02681-3

Muñoz-Sabater J, Dutra E, Agustí-Panareda A, et al (2021) ERA5-Land: a state-of-the-art global reanalysis dataset for land applications. Earth System Science Data 13(9):4349–4383. https://doi.org/10.5194/essd-13-4349-2021

Ohyama M, Hoshino Y, Yonenobu H, et al (2021) Chronology development of japanese cedar (*Cryptomeria japonica*) from the pacific ocean side of southern Tohoku. Bunkazai Kagaku 83:41–53. In Japanese with English title and summary; develops the MGNS (Sendai Castle Ninomaru cedar avenue) and MGDO (Daioji cedar avenue, Minamisanriku) reference chronologies for the Pacific side of southern Tohoku

Peltier DMP, Ogle K (2020) Tree growth sensitivity to climate is temporally variable. Ecology Letters 23(11):1561–1572. https://doi.org/10.1111/ele.13575

Shikoku Regional Forest Office (2008) Technical development completion report: Verification of growth-promotion effects of Yanase Sugi and related forests under warming trends. Tech. rep., Forestry Agency, Ministry of Agriculture, Forestry and Fisheries, Japan, Takamatsu, Japan, in Japanese; project period fiscal years 2006–2008; identifies the Yanase 2032 i41 compartment as the source of the analyzed stem discs

Shikoku Regional Forest Office (2024) Yanase Sugi. Tech. rep., Forestry Agency, Ministry of Agriculture, Forestry and Fisheries, Japan, Takamatsu, Japan, official management and conservation synthesis, in Japanese; summarizes domain-era forestry regulation, transfer to national-forest administration, and later conservation measures

Tei S, Nagai S, Sugimoto A (2019) Effects of climate dataset type on tree-ring analysis: A case study for siberian forests. Polar Science 21:136–145. https://doi.org/10.1016/j.polar.2018.10.008

Wasserstein RL, Lazar NA (2016) The ASA statement on P-values: context, process, and purpose. The American Statistician 70(2):129–133. https://doi.org/10.1080/00031305.2016.1154108

Yamanaka T (1954) Studies on the forest vegetation of Yanaze district, Shikoku, Japan. Research Reports of Kochi University 3(10):1–12. In Japanese with English summary

Yonenobu H, Hoshino Y, Ohyama M (2021) Yanase sugi (*cryptomeria japonica*) tree-ring chronology 1768–2004. Japanese Journal of Historical Botany 29(1):15–19

Yonenobu H, Ohyama M, Hoshino Y, et al (2026) Tree-ring evidence from a centuries-long plantation system: Growth trends and changing hydroclimatic sensitivity of japanese cedar in Yoshino, western Japan. Dendrochronologia 99:126572. https://doi.org/10.1016/j.dendro.2026.126572

Statements and Declarations

Funding

This work was supported by Japan Society for the Promotion of Science (JSPS) KAKENHI [grant numbers 25K00544 and 24H00118] to H.Y.; JSPS KAKENHI [grant number 25H00503] to Y.H.; JSPS KAKENHI [grant number 24K00152] to M.O.; and JSPS KAKENHI [grant number 24K04414] to G.K. The funders had no role in study design; data collection, analysis, or interpretation; preparation of the manuscript; or the decision to submit the work for publication.

Competing interests

The authors declare that they have no known competing financial interests or personal relationships that could have appeared to influence the work reported in this paper.

Author contributions

H.Y.: Conceptualization, data curation, formal analysis, funding acquisition, investigation, methodology, project administration, resources, software, supervision, validation, visualization, writing–original draft, writing–review and editing. K.Y.: Data curation, investigation, resources, validation, writing–review and editing. Y.H.: Data curation, formal analysis, investigation, validation, writing–review and editing. M.O.: Data curation, formal analysis, investigation, validation, writing–review and editing. G.K.: Formal analysis, investigation, validation, writing–review and editing.

Data and code availability

During peer review, editors and reviewers will have password-protected access to the Yanase code-and-data release assembled from the frozen R0 archive through Tohoku University's research-data service at https://nc.rdx.tohoku.ac.jp/s/z8fe5qWmLHxtjyx. Access credentials will be supplied to the editorial office separately. The package contains the 18-tree Yanase annual-ring data authorized for release, processed chronologies, derived climate variables and verification excerpts permitted for review, analysis scripts, deterministic settings, and frozen outputs needed to reproduce the reported results. The release also includes the versioned stand-coordinate CRU extraction, associated rerun analyses and coordinate-sensitivity comparisons, and the additional archived analyses reported here. Following acceptance, the release will be made openly and permanently available and assigned a DOI, which will be added to the accepted manuscript.

Japan Meteorological Agency observations, ERA5-Land, CRU TS, COBE-SST2, PDO, MEI.ext, NPI, AO, EASMI, and other third-party climate series remain available from their original providers and are not redistributed beyond the terms of those providers. Repository documentation gives source links and acquisition scripts where applicable. Fujiwara individual measurement data and internal repeat-measurement files are outside the submitted release.

Supplementary Files

This is a list of supplementary files associated with this preprint. Click to download.

- ESM1.pdf